Research Article Vol. 7, No. 5 / May 2020 / Optica 463

Ultrafast quantum photonics enabled by coupling plasmonic nanocavities to strongly radiative antennas

Simeon I. Bogdanov,[1,2,8,] Oksana A. Makarova,[1,2] Xiaohui Xu,[1,2] Zachariah O. Martin,[1,2] Alexei S. Lagutchev,[1,2] Matthew Olinde,[1,2] Deesha Shah,[1,2] Sarah N. Chowdhury,[1,2] Aidar R. Gabidullin,[3,4] Ilya A. Ryzhikov,[3,5] Ilya A. Rodionov,[3,4] Alexander V. Kildishev,[1,2] Sergey I. Bozhevolnyi,[6] Alexandra Boltasseva,[1,2] Vladimir M. Shalaev,[1,2] and Jacob B. Khurgin[7]

[1]School of Electrical Computer Engineering, Purdue University, West Lafayette, Indiana 47907, USA
[2]Purdue Quantum Science and Engineering Institute, Purdue University, West Lafayette, Indiana 47907, USA
[3]FMN Laboratory, Bauman Moscow State Technical University, Moscow 105005, Russia
[4]Dukhov Automatics Research Institute (VNIIA), Moscow 127055, Russia
[5]Institute for Theoretical and Applied Electromagnetics RAS, Moscow 125412, Russia
[6]Centre for Nano Optics, University of Southern Denmark, Campusvej 55, DK-5230 Odense M, Denmark
[7]Johns Hopkins University, Baltimore, Maryland 21218, USA
[8]Department of Electrical and Computer Engineering, University of Illinois at Urbana-Champaign, Urbana, Illinois 61801, USA
*Corresponding author: bogdanov@illinois.edu

Received 21 November 2019; revised 30 March 2020; accepted 30 March 2020 (Doc. ID 382841); published 7 May 2020

Quantum emitters coupled to plasmonic nanostructures can act as exceptionally bright sources of single photons, operating at room temperature. Plasmonic mode volumes supported by these nanostructures can be several orders of magnitude smaller than the cubic wavelength, which leads to dramatically enhanced light–matter interactions and drastically increased photon production rates. However, when increasing the light localization further, these deeply subwavelength modes may in turn hinder the fast outcoupling of photons into free space. Plasmonic hybrid nanostructures combining a highly confined cavity mode and a larger antenna mode circumvent this issue. We establish the fundamental limits for quantum emission enhancement in such systems and find that the best performance is achieved when the cavity and antenna modes differ significantly in size. We experimentally support this idea by photomodifying a nanopatch antenna deterministically assembled around a nanodiamond known to contain a single nitrogen–vacancy NV) center. As a result, the cavity mode shrinks, further shortening the NV fluorescence lifetime and increasing the single-photon brightness. Our analytical and numerical simulation results provide intuitive insight into the operation of these emitter–cavity–antenna systems and show that this approach could lead to single-photon sources with emission rates up to hundreds of THz and efficiencies close to unity.

https://doi.org/10.1364/OPTICA.382841

1 INTRODUCTION

Solid-state quantum emitters (QEs) are key elements of future quantum communication and information processing technologies as sources of single photons [1]. One of their major drawbacks compared to nonlinear optical single-photon sources [2] is the fast, pure dephasing of the emitting optical dipoles. In the optical range, the vacuum spontaneous emission rate of QEs is naturally limited to about 1 GHz due to a highly subwavelength dipole moment. Pure dephasing, especially at non-cryogenic temperatures occurs much faster, making the single-photon emission incoherent and inapplicable to coveted multi-photon interference operations. Strongly accelerating the photon emission rate therefore constitutes a major task on the way to implementing high-speed efficient quantum networks [3–7].

The speed-up of the photon emission rate can be achieved by increasing the density of photon states at the emitter transition energy with the help of resonant optical nanostructures. This effect shortens the emitter excited state lifetime and yields a higher emitted photon rate. It can be achieved in either high-Q dielectric cavities with diffraction-limited mode volumes, or in low-Q plasmonic structures with sub-diffraction mode volumes. Previously [8,9], it has been shown that despite the relatively low Q of plasmonic modes, the radiation rate of a QE in the proximity of an aspherical nanoparticle can be higher than in dielectric photonic

cavities, reaching the THz range. The upper limit on the radiative plasmonic enhancement was found to be two orders of magnitude higher than that in dielectric cavities. We show here that it is possible to significantly exceed the previously established limit for plasmonic cavities. This result opens possibilities for circumventing strong absorption losses in plasmonic nanostructures and dipole dephasing in matter.

In the simplest plasmonic resonators based on a single metallic particle, the particle simultaneously plays two roles. It serves as a resonant cavity, which provides a high local density of plasmonic states. At the same time, it is responsible for coupling the plasmons to the far field, behaving as an antenna. In accordance with this, the volume of the nanoparticle needs to be optimized so that it is sufficiently small to produce a large excited state lifetime shortening, yet at the same time large enough to efficiently couple plasmons into the outer space. The requirements of a small mode volume for stronger confinement and a sufficiently large volume for an efficient outcoupling are contradictory and cannot be met in a simple structure, such as a single nanoparticle. One can instead follow the path that is routinely chosen in electronics, namely, use separate entities for resonant cavity and antenna that are efficiently coupled to each other. For our photonic scenario, this approach implies coupling a small volume plasmonic cavity with a larger plasmonic mode serving as a nanoantenna. One such solution involving a plasmonic dimer with two nanospheres of different radii has been investigated theoretically [10]. Many other examples have been demonstrated [11–13] involving dipole [14], bowtie [15] and nanopatch antennas (NPAs) [16,17], and hybrid dielectric loaded antennas [18].

The majority of demonstrated gap plasmon-based single-photon nanoantennas operate far from their fundamental limits dictated by the material and geometric parameters. Here, we show that the emission enhancement in the NPA configuration, in which the roles of the cavity and antenna are played by the gap and the nanocube, respectively, can be improved using a simple photomodification technique. As a result of the photomodification, the effective cavity volume is reduced (Fig. 1). The reduction in cavity volume boosts both the total decay rate and the detected photon rate. We develop a simple analytical approach to explain these results and confirm them with numerical simulations. Using the analytical model, we estimate the maximum radiative rate enhancement attained using nanophotonic elements that combine cavities and antennas with optimal sizes. We find that the maximum theoretically predicted radiative rate enhancement strongly depends on the cavity and antenna mode volumes. This enhancement factor can reach over a million times while maintaining near-unity efficiency for realistic emitter and nanostructure parameters.

2 CONTROLLING THE CAVITY MODE VOLUME

Nanostructures made of soft metals such as gold and silver can be modified while exposed to intense incident light such as one produced by a focused laser. Previously, light-induced geometry modification has been shown to affect the optical properties of plasmonic nanostructures. It is often an unwanted phenomenon that degrades the nanostructure performance [19,20]. In some cases, however, it may help the shaping of desired nanostructures as in the case of laser-written metasurfaces [21]. One commonly observed consequence of laser treatment is the sintering in metallic particles, and the modification of their far-field optical response including scattering of light [22]. The near-field behavior has been observed to change as well [23].

We performed an experiment using a deterministically assembled [24] NPA [Fig. 1(a)] formed by a crystalline silver nanocube and an epitaxial SCULL (single-crystalline continuous ultrasmooth low-loss low-cost) silver film [25]. A nanodiamond with 17 nm height hosting a single nitrogen–vacancy (NV) center was first identified on a glass coverslip substrate, optically characterized, then transferred to the silver film by means of an atomic force microscope tip and coated with a 5 nm thick alumina spacer layer. Finally, silver nanocubes were drop casted onto the silver sample. One of them was deterministically pushed over the nanodiamond, embedding the latter into the plasmonic gap of the resulting NPA. In the past, such structures have been demonstrated to speed up the excited state decay rate dramatically [16] and exhibit high radiation efficiency [17]. The cavity volume is defined by the space between the cube and the underlying metal film. This volume consists of three parts: the spacer layer in the gap, the diamond nanoparticle, and the air gap resulting from the elevation of the cube by the nanoparticle. The air gap initially took up the majority of the cavity volume. The subsequent sintering of the cube during the laser treatment led to the shrinking of the air gap and thereby to a reduction of the plasmonic cavity volume. The plasmonic antenna volume, however, remained largely the same.

The NPA with an embedded NV center was characterized first directly after its assembly, then after an intense optical treatment. To modify the NPA, we subjected it to a prolonged 30 s illumination with a 1 mW continuous-wave laser beam at 532 nm. The structure experienced an incident power density of about $3 \cdot 10^4$ W/cm^2, a level comparable to that used previously for optical NPA deformation [20]. In a reference experiment, we recorded an average nanocube height change of 1.9 ± 0.7 nm over

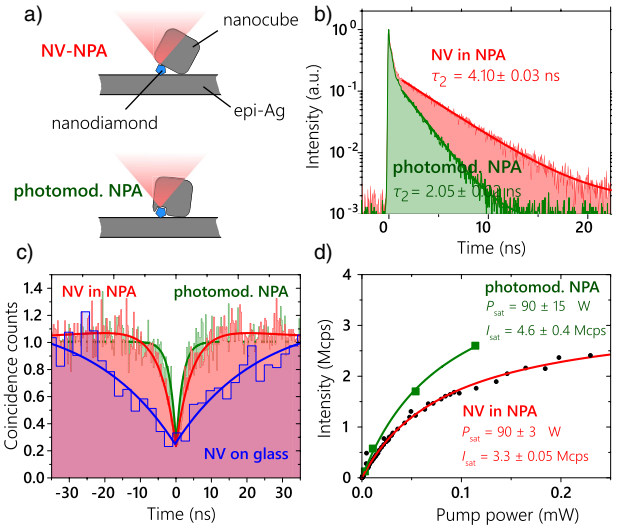

Fig 1 Photomodification of a nanopatch antenna with an embedded single nitrogen–vacancy center in a nanodiamond. (a) Schematics of the nanopatch antenna before and after photomodification. (b) NV center fluorescence lifetime changes as a result of nanopatch antenna photomodification. (c) Photon antibunching of the NV photoluminescence is conserved during photomodification (red and green curves; data measured at an incident pump power of 3 W). The antibunching data for the same NV center on glass substrate prior to NPA assembly is shown in blue (data measured at an incident pump power of 340 W). (d) Photoluminescence saturation curves illustrate that NV brightness increases after photomodification.

five randomly assembled antennas as a result of this procedure (see Supplement 1 for details). Because the field is maximal in the gap between the cube and the silver film, it is also where one expects the largest geometric changes to occur.

The emitter behavior changes substantially after the NPA photomodification. The photoluminescence decay measurements [Fig. 1(b)] featured bi-exponential decay curves likely due to the combination of slower emitter fluorescence with a faster background emission. Before and after NPA photomodification, the characteristic times τ_2 of the slower decay components were 4.10 ± 0.03 ns and 2.05 ± 0.02 ns, respectively. We confirmed that these slower components correspond to the fluorescence of a single NV center by performing autocorrelation measurements under constant pump intensity [Fig. 1(c)]. Remarkably, the single-photon purity of the NV was not affected by the photomodification procedure. The autocorrelation dip, however, became narrower, in good agreement with the pulsed measurements of the excited state decay. Finally, by measuring fluorescence intensity at different laser powers, we found that the NV brightness was further improved as a result of NPA photomodification. The retrieved saturation intensity increased from 3.3 to 4.6 Mcps [Fig. 1(d)]. This increase in the brightness points to the fact that the twofold decay rate enhancement was in substantial part due to the faster radiative decay rate into the cavity mode.

In order to confirm the reproducibility of the photomodification effect, we assembled additional NPAs by randomly casting nanodiamonds and nanocubes onto the silver substrate. Some of these particles spontaneously arranged into single-photon NPAs [17] that we characterized before and after the same photomodification procedure. The optical characterization results are available in Supplement 1.

3 EFFECTIVE CAVITY VOLUME AND EFFECTIVE DIPOLE: ANALYTICAL TREATMENT

We now propose a simple analytical model that explains how a controllable reduction of cavity volume improves the single-photon source performance. We extend our analysis performed in Ref. [8] to the general plasmonic cavity/antenna combination and show that an additional order of magnitude enhancement relative to a single plasmonic nanoparticle is attainable. Furthermore, the ever-present nonradiative loss associated with plasmonic materials can be substantially reduced if the photons exit the antenna before they get absorbed by the metal.

Let us consider two strongly coupled modes a_1 and a_2 with the same resonance frequency and a quantum dipole resonating at a frequency ω and linewidth $\Delta\omega$. In the NPA configuration, the cavity mode is the gap mode between the cube and the metallic film, while the cube itself plays the role of the antenna [Fig. 1(a)]. The metal is optically characterized by its plasma frequency ω_p and its plasmon absorption rate γ_{ohm}. For a nanoantenna made of crystalline silver, we take $\gamma_{\mathrm{ohm}} = 2\pi \times 2$ THz and $\omega_p = 2\pi \times 2200$ THz [25,26]. We assume that the smaller cavity mode has an effective volume V_1, while the larger antenna mode has a volume V_2. When the modes are strongly coupled, i.e., the coupling rate κ exceeds the total energy loss rate $\gamma_{\mathrm{ohm}} + \gamma_{\mathrm{rad}}$, the energy is equally distributed between two modes, i.e., a coupled mode $a_+ = (a_1 + a_2)/\sqrt{2}$ with resonant frequency ω_+ is formed, as shown in Fig. 2(b). We assume that the nanopatch system is built in such a way that the ground hybridized mode is resonant with the quantum dipole ($\omega_+ = \omega$). In addition, a second coupled mode $a_- = (a_1 - a_2)/\sqrt{2}$ may be formed, but as long as $\Delta\omega < \kappa$, its frequency $\omega_- \approx \omega_+ + 2\kappa$ is sufficiently detuned from the quantum dipole.

Let us calculate the far-field photon radiation rate γ_{ff} in the optical saturation regime. The interaction of our dipole with free space is mediated through the mode a_+. The dipole has a vacuum radiative decay rate γ_0, but in our system, it transfers its excitation to a_+ at a rate γ_{tr}. At the same time, it suffers from an intrinsic non-radiative decay rate γ_{nr}, leading to a finite quantum yield $QY = \gamma_{\mathrm{tr}}/(\gamma_{\mathrm{tr}} + \gamma_{\mathrm{nr}})$. The spontaneous rate enhancement provided by the antenna is usually very large ($\gamma_{\mathrm{tr}} \gg \gamma_{\mathrm{nr}}$). Therefore, in what follows, we will neglect the non-radiative rate. Instead, we assume an ideal quantum dipole with an intrinsic radiative rate of $\gamma_0 = 100$ MHz emitting at a frequency of $\omega = 2\pi \times 400$ THz corresponding to a free-space wavelength of $\lambda = 700$ nm.

The hybrid mode in turn radiates the plasmon into the far field at a rate γ_{rad} and loses it to heat at a rate γ_{ohm}. We summarize the interplay of these pathways in Fig. 2(b). From this scheme, we can express the desired quantity as $\gamma_{\mathrm{ff}} = \gamma_{\mathrm{tr}}\eta_{\mathrm{rad}}$, where $\eta_{\mathrm{rad}} = \gamma_{\mathrm{rad}}/(\gamma_{\mathrm{rad}} + \gamma_{\mathrm{ohm}})$ is the hybrid mode's radiation efficiency.

To estimate γ_{ff}, we first determine γ_{tr} and γ_{rad} as a function of the mode's geometric parameters. The hybrid mode a_+ simultaneously acts as an antenna and as a cavity. The enhancement of the quantum dipole radiation rate is characterized by the effective antenna and cavity volumes, which are not equal to each other for a_+ because of its hybridized nature. The uncoupled modes a_1 and a_2 have volumes V_1 and V_2, respectively. The coupling of these modes gives rise to an effective antenna volume V_A and an effective cavity volume V_C for the mode a_+. We normalize these volumes by the diffraction volume $V_0 = 3\lambda^3/4\pi^2 n^3$. In the rest of the text, we utilize the normalized volumes $v_A = V_A/V_0$, $v_C = V_C/V_0$, $v_1 = V_1/V_0$, and $v_2 = V_2/V_0$.

The radiative antenna rate can be directly assessed as $\gamma_{\mathrm{rad}} = v_A \omega_p^2/\omega$ (see Supplement 1). This expression agrees with the intuitive picture of the plasmon decay as the superradiance from all of its constituent electrons. Since the superradiant decay rate must scale with the number of phased dipoles, the plasmonic antenna radiative rate therefore is proportional to the electronic density times the mode volume.

Combining the radiative loss rate with the ohmic loss rate γ_{ohm}, we obtain the total hybrid mode's quality factor as $Q_+ = \omega/(\gamma_{\mathrm{rad}} + \gamma_{\mathrm{ohm}})$. The emitter transfer rate can be now expressed through the enhancement factor $\gamma_{\mathrm{tr}} = \gamma_0 F_+ = \gamma_0 Q_+/v_C$. Finally, we arrive at the enhancement of the far-field photon production rate expressed in terms of the geometric and material parameters of the nanostructure:

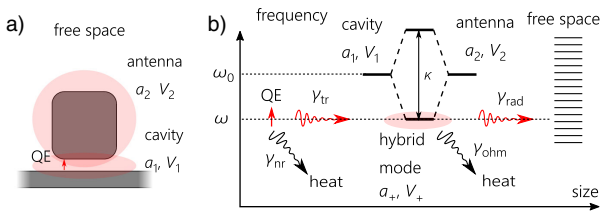

Fig 2 (a) Nanopatch antenna viewed as a cavity–antenna system enhancing the emission from a quantum emitter coupled to the gap plasmonic cavity; (b) formation of the coupled mode and the diagram of energy flow in a cavity–antenna system.

$$\frac{\gamma_{\rm ff}}{\gamma_0} = \frac{\omega_p^2}{\gamma_{\rm ohm}^2} \frac{v\ /v_C}{\left(1 + v\ \frac{\omega_p^2}{\gamma_{\rm ohm}\omega}\right)^2}, \tag{1}$$

where $v\ (v_1, v_2) = (\sqrt{v_1} + \sqrt{v_2})^2/2$, and $v_C(v_1, v_2) = 2v_1$. We briefly justify the expressions for these mode volumes. a_+ as a superposition mode is characterized by the fact that the energy spends only half of the time in a_1 and half of the time in a_2. Simplistically, if one assumes that the emitter does not couple directly to a_2, and a_1 does not radiate, then a_+ is only half as effective as a_1 in terms of its performance as a cavity and half as effective as a_2 in terms of its antenna performance. Therefore, in the limit $v_1 \ll v_2$, we have $v\ \approx v_2/2$ and $v_C = 2v_1$. A more exact derivation can be found in Supplement 1.

The far-field photon production rate $\gamma_{\rm ff}$ is furthermore limited by several conditions. The cavity and antenna volumes are constrained by our assumption that they are strongly coupled. According to references [11,12], the coupling rate between the cavity and the antenna caused by dipole–dipole interaction is roughly $\kappa \sim \omega V_1^{1/2} V_2^{1/2}/r_{12}^3$, where r_{12} is the distance between dipoles. The exact expression of the distance between the modes depends on the details of the nanostructure geometry, but in the case of an NPA, we have $r_{12}^3 \sim V_2/8$. For the case of $V_2 \gg V_1$ the condition of strong coupling between a_1 and a_2 simply becomes $256\ ^2v_1 > v_2(\beta v_2 + 2)^2$, where $= \omega/\gamma_{\rm ohm}$, and $\beta = \omega_p^2\omega\ ^1\gamma_{\rm ohm}^{\ 1}$. In practice, even if the strong coupling regime is not actually achieved, the energy will still be shared between the (dark) cavity mode and the (bright) antenna mode simply because the latter's radiative efficiency is much stronger. Transferring energy to the antenna mode will therefore still lead to additional emission enhancement, although at a level deviating from the optimum. We must also demand that the emitter is not strongly coupled to the cavity ($\gamma_{\rm rad} + \gamma_{\rm ohm} > \gamma_{\rm tr}$). This condition leads to an additional geometric constraint: $v_C(\beta v\ + 1)^2 > \delta$, where $\delta = \omega\gamma_0/\gamma_{\rm ohm}^2$. With these notations, the radiative efficiency $\eta_{\rm rad}$ can be simply expressed as $\eta_{\rm rad} = (1 + \beta\ ^1v\ ^1)\ ^1$.

In Fig. 3, we plot the far-field photon production rate in plasmonic emitter–cavity–antenna systems along with the aforementioned constraints as a function of the normalized volumes v_1 and v_2. For the cavity–antenna strong coupling limit, the approximation $V_2 \gg V_1$ indeed applies well within our parameter space and admits the analytical expression above. However, as it comes to the emitter–cavity strong coupling limit, this approximation does not generally hold, and a numerical solution expressing v_1 as a function of v_2 must be used.

We now calculate the far-field photon production rate and radiation efficiency corresponding to the optimally chosen mode volumes. Directly from the map in Fig. 3, we extract $\gamma_{\rm ff}^{\rm opt}/\gamma_0 \approx 3 \cdot 10^6$ and $\eta_{\rm rad}^{\rm opt} \approx 96$, corresponding to physical mode volumes of $V_1 \approx (3\,{\rm nm})^3$ and $V_2 \approx (60\,{\rm nm})^3$. The absolute optimal free-space photon production rate is as high as $\gamma_{\rm ff}^{\rm opt} \approx 300$ THz. With the assumptions of strongly dissimilar mode sizes ($V_2 \gg V_1$) and high radiative efficiency ($\beta v_2 \gg 2$), the expressions for the optimal enhanced photon emission rate and the radiative efficiency become analytical:

$$\gamma_{\rm ff}^{\rm opt} \approx 1.7\ \omega_p^2\omega^2\gamma_0)^{1/5},\ \eta_{\rm rad}^{\rm opt} \approx 1\ \ \frac{\gamma_{\rm ohm}}{\gamma_{\rm ff}^{\rm opt}} \tag{2}$$

and yield quantitative results that are very similar to those extracted from the map. This result suggests that quantum dipoles coupled to hybridized plasmonic nanocavities may be capable of producing a photon within a few cycles of the optical field and with near-unity efficiency. In the case of an enhancing structure consisting of a single plasmonic nanoparticle [8], the optimum photon production rate is $\gamma_{\rm ff}^{\rm 1NP} = 0.25\gamma_0(\omega_p/\gamma_{\rm ohm})^2 \sim 30$ THz with an efficiency of $\eta_{\rm rad}^{\rm 1NP} = 50$. We note that the above numerical estimates correspond to the choice of low-loss crystalline silver as the plasmonic metal. These estimates exhibit ω_p as the essential material parameter when it comes to considering other metals. The plasma frequency ultimately limits the photon production rate, even as losses become negligible. At the same time, $\gamma_{\rm ff}^{\rm opt}$ depends weakly on the intrinsic emission rate γ_0. One would need to employ a more rigorous approach to quantify the decay rates near plasmonic nanostructures more precisely [27–30]. However, our order-of-magnitude analysis provides intuitive insight into the operation of emitter–cavity–antenna systems without involving the full-wave simulations presented below or more complex analytical methods.

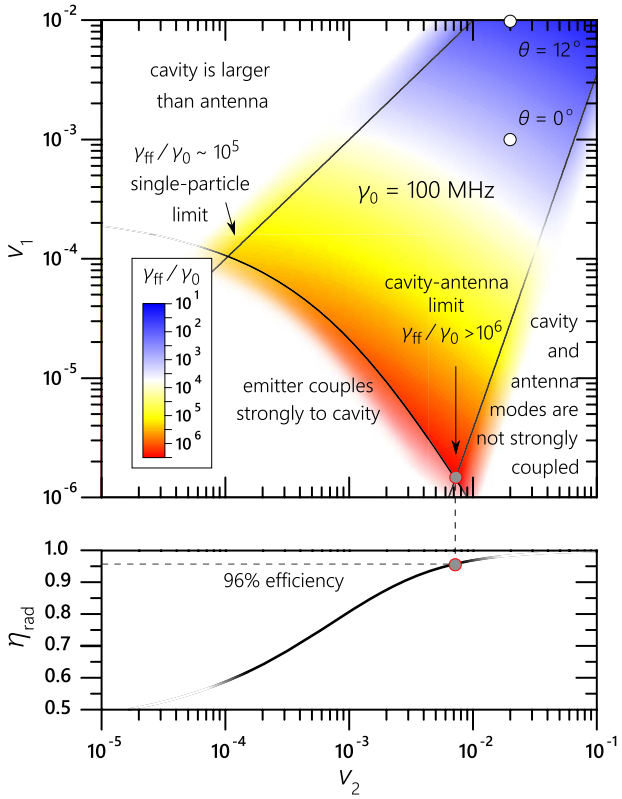

Fig 3 (a) $\gamma_{\rm ff}/\gamma_0$ for a quantum emitter with unity internal quantum yield coupled to a plasmonic cavity–antenna system as a function of the normalized unitless mode volumes v_1 and v_2. Continuous black lines correspond to the different validity limits of our analytical description. Whitened areas represent phase space regions where our assumptions break down. The emitter–cavity strong coupling condition is plotted for $\gamma_0 = 100$ MHz. The gray circle in the bottom of the map denotes the optimal point in the phase space (v_1, v_2) within the validity limits. White circles correspond to the numerically simulated cases of nanopatch antennas with nanocube inclination angles of 10.7° and 0°. (b) Radiative efficiency $\eta_{\rm rad}$ plotted along the emitter–cavity strong coupling limit.

4 NUMERICALLY SIMULATED PERFORMANCE OF PHOTOMODIFIED NANOPATCH ANTENNAS

We now show numerically that the above coupled mode analysis adequately describes the behavior of NPAs as their cavity volume is scaled down through photomodification. We first simulated the

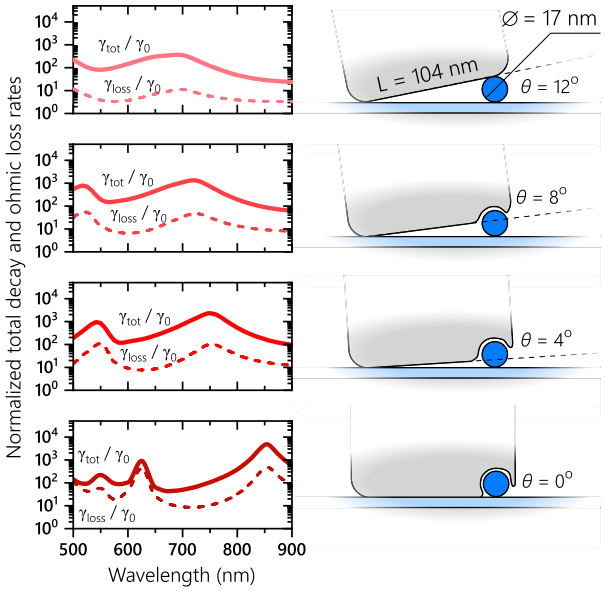

Fig 4 Simulations of total decay rate (solid lines) and total ohmic loss rates (dashed lines) for a quantum emitter in nanodiamond coupled to a progressively modified NPA. Four different NPA configurations are simulated corresponding to different degrees of photomodification labeled by the values of nanocube inclination angle θ.

performance of the NPA as it was assembled (Fig. 4). The nanodiamond was assumed to be spherical with a diameter of 17 nm; the nanocube's side was 110 nm, and the spacer thickness was 5 nm. The nanodiamond was sitting under one of nanocube's corners. The dipole was assumed to be vertically oriented and located in the center of the nanodiamond. The cube's lower surface formed an angle of $\theta = 12°$ with the underlying silver film's surface. We then modeled the performance of a photomodified NPA by progressively reducing the angle θ to zero. At the same time, the lower surface of the nanocube was curved to accommodate the undeformable nanodiamond. All the simulated rates are normalized to the radiative rate $\gamma_0 = 10$ MHz, corresponding to that of an NV center in a 17 nm nanodiamond on a glass substrate with index $n_g = 1.5$. We simulated the total decay rates $\gamma_{tot} = \gamma_{nr} + \gamma_{tr}$ of emitters coupled to the NPA as well as the rate of ohmic loss γ_{loss}. The ohmic loss rate was obtained by integrating the rate of energy absorption over the entirety of the metallic structure. As θ changes, the NPA resonance wavelength shifts. In order to obtain the resonant decay and loss rates, γ_{tot} and γ_{loss} were simulated over a range of wavelengths between 500 nm and 900 nm. More details on the simulation methods and definitions are available in Supplement 1.

As the cavity volume was progressively reduced, we observed an increase in the peak total decay rates at the wavelengths of cavity resonances. The fundamental resonance occurred at $\lambda = 670$ nm for the unmodified cavity ($\theta = 12°$) as the nanocube touched the tip of the nanodiamond. The resonance red shifted to 860 nm for $\theta = 0°$ configuration, as the nanocube lay flat on the spacer film. The corresponding total decay rate enhancement at resonance increased from nearly 400 times to about 5000 times. In all the configurations, the ohmic loss rate at the fundamental resonance remained well below the total decay rate. This relatively low ohmic loss indicates that the decay enhancement is mostly radiative in nature. In accord with the analytical model, the reduction of cavity volume leads to an increase in the rate of single-photon production.

We note that for our hypothesis of equal energy sharing between the cavity and antenna modes, they must exhibit a strong spectral overlap, also maximizing the radiation efficiency. In practice, this spectral matching may be achieved by choosing an appropriate nanocube size for a given gap volume. The spectral matching is greatly facilitated by the low antenna quality factor.

To compare these results to our experimental outcome, we average the rates over the wavelength range of 600–700 nm, corresponding to the emission range of the NV centers. Between the first two configurations ($\theta = 12°$ and $\theta = 8°$), we record an increase in the averaged normalized total decay rate by almost a factor of two (300 and 550 times, respectively). The loss rates in both cases account for less than 3 of the total decay rate. This high radiative efficiency is a consequence of the large volume of the antenna mode ($v_2 \approx 0.02$; see Supplement 1 for details). In the photomodification experiment, we recorded a commensurate increase in fluorescence rate. The fluorescence lifetime shortening in our experiment is smaller than in the idealized numerically simulated case (about 12 and 25 before and after photomodification, respectively). This is presumably due to the finite NV center's intrinsic quantum yield [31], a random NV dipole orientation, suboptimal positioning of the nanodiamond with respect to the nanocube, and an imperfect spectral overlap between the emitter dipole and the NPA resonance. In practice, emission rate enhancements of 100 times are achievable in randomly assembled NPAs [17], and a fluorescence lifetime shortening of over 1000 can be observed using optimal assembly of the NPAs [24] (see Supplement 1 for a detailed numerical study of dipole position in the NPA). We anticipate that approaching theoretically optimal results may be possible using color centers with higher quantum yield [32], crystalline diamond membrane hosts for better control of dipole orientation, [33] and subwavelength emitter localization [34] to facilitate optimal nanocube positioning.

We also compare this result to the analytical estimates plotted in Fig. 3. For this purpose, we calculate the antenna and cavity mode volumes. While the nanocube volume is kept at $v_2 \approx 0.02$, the cavity volume is progressively scaled from $v_1 \approx 1.4 \cdot 10^{2}$ to $1.0 \cdot 10^{3}$ (see Supplement 1 for details). The corresponding points on the volume phase space are marked in Fig. 3. The corresponding analytical estimate for $\theta = 12°$ (0°) gives a total decay rate enhancement of about 150 times (3000 times). These numbers are computed by normalizing the decay rates to those of a dipole located in a nanodiamond on glass substrate, as in the numerical simulation. It indicates that our analytical theory provides a theoretical limit for the given cavity and antenna mode volumes that is commensurate with the performance of a NPA. The remaining discrepancy between the analytical and numerical calculations can be attributed to the rough estimate of the cavity mode volume and to neglecting the influence of dielectrics in the cavity with a refractive index greater than one [35].

5 DISCUSSION

We have systematically studied coupled systems of QEs, ultrasmall plasmonic cavities and larger nanoantennas. We explored their strong ability to enhance the radiative QE emission rate and efficiently outcouple the plasmon excitations into free space. These structures combine a small effective volume with a large effective dipole and thus serve simultaneously as small cavity and large antenna elements. The two modes must coexist at the same frequency and couple strongly. A detailed study of the effect of the

cavity and antenna mode hybridization was published during the preparation of this paper [30]. We explored the limits of the fluorescence rate enhancement using very generalized arguments that can be applied to any shape of the nanostructure under study. This analysis is readily extendable to the study of nanostructures consisting of more than two matching elements, such as the recently reported gap plasmon antennas with "picocavities" [36]. We theoretically showed that the QE rate may reach values as high as hundreds of THz. Our study provides a practical route to achieving efficient ultrafast single-photon emission at non-cryogenic temperatures with a strong promise of achieving efficient generation of indistinguishable photons in the near future.

If such high emission rates are achieved, one must ensure that the emitter is pumped into the excited state with a rate even higher than its decay rate, which appears to be problematic due to several practical reasons [29]. Whether the plasmonic electron motion will contribute to dipole dephasing in ultra-small plasmonic cavities remains to be studied. However, the geometric and material requirements for beating the typical dephasing rates in QEs at cryo-free temperatures [37] appear to be realistic. The physical mode volumes at which the optimum far-field production rate occurs are $V_1 \approx (3\,\mathrm{nm})^3$ and $V_2 \approx (60\,\mathrm{nm})^3$. These mode volumes are compatible with emitters such as nanodiamond-based color centers. For example, single fluorescing SiV centers with narrow linewidths below 10 nm have been previously found in meteoritic nanodiamonds with sizes as small as 2 nm [38]. We note that combining the plasmonic cavity–antenna systems with larger dielectric cavities can alleviate the ultra-small mode volume requirements to achieve similar enhancement [39].

One can alternatively think of the emitter–cavity–antenna combination as a two-stage impedance-matching circuit between a high-impedance emitter and a low-impedance free-space mode. A previous analysis, based on calculating antenna impedance for plasmonic dimer antennas made of conventional gold [14] indicated that gaps smaller than 10 nm could not be reached without a significant loss in efficiency. That estimate led to the maximum enhancement factor of a few thousand before the efficiency dropped below 50 . We note that the material parameters of crystalline silver are crucial in making 100 THz emission rates possible. Using our analysis, we can attribute the exceptional theoretical performance of silver cavity–antennas to the high plasma frequency and a low ohmic loss rate. At the same time, a dimer antenna is more extended spatially than an NPA of the same volume. Therefore, in a dimer antenna, the effective distance between the antenna and cavity mode locations is longer, and the cavity–antenna strong coupling condition is more restrictive on the cavity mode volume.

We have further validated the analytical picture using numerical and experimental methods. In both cases, we have observed an improvement in the NPA performance with the downscaling of the cavity mode volume. It is important to note that according to Fig. 1(d), it is mostly the radiative decay that is enhanced rather than nonradiative decay near the surface of the metal, commonly referred to as "photoluminescence quenching." Quenching normally occurs when the energy of the emitter becomes coupled into the higher-order nonradiative plasmonic modes localized very close to the metal surface, so the energy of these modes decays nonradiatively into the electron hole pairs in the metal [40]. The effect of quenching in the limit of very small gaps can be estimated from the efficiency of coupling to the gap–plasmon mode $\beta_{\mathrm{SPP}} \approx (1 + \mathrm{Im}\varepsilon_m/2)^{-1}$ [35], provided that the QE is in the middle of the gap. Quenching can therefore be disregarded when making order-of-magnitude estimations for visible wavelengths. Moreover, in the cavity–antenna geometry with low spatial symmetry, the higher-order modes are also coupled to the antenna modes and can be radiated rather than dissipated within the metal [41].

Funding Department of Energy, Office of Basic Energy Sciences, Division of Materials Sciences and Engineering (DE-SC0017717) (Purdue co-authors SIB, AB and VMS); Air Force Office of Scientific Research (FA9550-16-10362); DARPA Defense Sciences Office (HR00111720032).

Acknowledgment Epitaxial silver samples were deposited at the BMSTU Nanofabrication Facility (Functional Micro/Nanosystems, FMNS REC, ID 74300). The authors thank Scott Jordan from Physik Instrumente for his assistance with the automation and control of the piezoelectric microscope stage.

Disclosures The authors declare no conflicts of interest.

See Supplement 1 for supporting content.

REFERENCES

1. I. Aharonovich, D. Englund, and M. Toth, "Solid-state single-photon emitters," Nat. Photonics **10**, 631–641 2016).
2. L. Caspani, C. Xiong, B. J. Eggleton, D. Bajoni, M. Liscidini, M. Galli, R. Morandotti, and D. J. Moss, "Integrated sources of photon quantum states based on nonlinear optics," Light: Sci. Appl. **6**, e17100 2017).
3. S. I. Bogdanov, A. Boltasseva, and V. M. Shalaev, "Overcoming quantum decoherence with plasmonics," Science **364**, 532–533 2019).
4. S. Wein, N. Lauk, R. Ghobadi, and C. Simon, "Feasibility of efficient room-temperature solid-state sources of indistinguishable single photons using ultrasmall mode volume cavities," Phys. Rev. B **97**, 205418 2018).
5. Y. Luo, X. He, Y. Kim, J. L. Blackburn, S. K. Doorn, H. Htoon, and S. Strauf, "Carbon nanotube color centers in plasmonic nanocavities: a path to photon indistinguishability at telecom bands," Nano Lett. **19**, 9037–9044 2019).
6. Y. Luo, G. D. Shepard, J. V. Ardelean, D. A. Rhodes, B. Kim, K. Barmak, J. C. Hone, and S. Strauf, "Deterministic coupling of site-controlled quantum emitters in monolayer WSe 2 to plasmonic nanocavities," Nat. Nanotechnol. **13**, 1137 2018).
7. T. T. Tran, D. Wang, Z.-Q. Xu, A. Yang, M. Toth, T. W. Odom, and I. Aharonovich, "Deterministic coupling of quantum emitters in 2D materials to plasmonic nanocavity arrays," Nano Lett. **17**, 2634–2639 2017).
8. S. I. Bozhevolnyi and J. B. Khurgin, "Fundamental limitations in spontaneous emission rate of single-photon sources," Optica **3**, 1418–1421 2016).
9. S. I. Bozhevolnyi and J. B. Khurgin, "The case for quantum plasmonics," Nat. Photonics **11**, 398–400 2017).
10. G. Sun and J. B. Khurgin, "Theory of optical emission enhancement by coupled metal nanoparticles: an analytical approach," Appl. Phys. Lett. **98**, 113116 2011).
11. K. Li, M. I. Stockman, and D. J. Bergman, "Self-similar chain of metal nanospheres as an efficient nanolens," Phys. Rev. Lett. **91**, 227402 2003).
12. P. Nordlander, C. Oubre, E. Prodan, K. Li, and M. I. Stockman, "Plasmon hybridization in nanoparticle dimers," Nano Lett. **4**, 899–903 2004).
13. S. K. H. Andersen, S. Kumar, and S. I. Bozhevolnyi, "Ultrabright linearly polarized photon generation from a nitrogen vacancy center in a nanocube dimer antenna," Nano Lett. **17**, 3889–3895 2017).
14. M. S. Eggleston, K. Messer, L. Zhang, E. Yablonovitch, and M. C. Wu, "Optical antenna enhanced spontaneous emission," Proc. Natl. Acad. Sci. USA **112**, 1704–1709 2015).

15. A. Kinkhabwala, Z. Yu, S. Fan, Y. Avlasevich, K. Müllen, and W. E. Moerner, "Large single-molecule fluorescence enhancements produced by a bowtie nanoantenna," Nat. Photonics **3**, 654–657 2009).
16. T. B. Hoang, G. M. Akselrod, and M. H. Mikkelsen, "Ultrafast room-temperature single photon emission from quantum dots coupled to plasmonic nanocavities," Nano Lett. **16**, 270–275 2016).
17. S. I. Bogdanov, M. Y. Shalaginov, A. S. Lagutchev, C.-C. Chiang, D. Shah, A. S. Baburin, I. A. Ryzhikov, I. A. Rodionov, A. V. Kildishev, A. Boltasseva, and V. M. Shalaev, "Ultrabright room-temperature sub-nanosecond emission from single nitrogen-vacancy centers coupled to nanopatch antennas," Nano Lett. **18**, 4837–4844 2018).
18. Y. Yang, O. D. Miller, T. Christensen, J. D. Joannopoulos, and M. Soljačić, "Low-loss plasmonic dielectric nanoresonators," Nano Lett. **17**, 3238–3245 2017).
19. G. Albrecht, S. Kaiser, H. Giessen, and M. Hentschel, "Refractory plasmonics without refractory materials," Nano Lett. **17**, 6402–6408 2017).
20. A. Kuhlicke, S. Schietinger, C. Matyssek, K. Busch, and O. Benson, "In situ observation of plasmon tuning in a single gold nanoparticle during controlled melting," Nano Lett. **13**, 2041–2046 2013).
21. S. V. Makarov, V. A. Milichko, I. S. Mukhin, I. I. Shishkin, D. A. Zuev, A. M. Mozharov, A. E. Krasnok, and P. A. Belov, "Controllable femtosecond laser-induced dewetting for plasmonic applications," Laser Photon. Rev. **10**, 91–99 2016).
22. J. Mertens, M.-E. Kleemann, R. Chikkaraddy, P. Narang, and J. J. Baumberg, "How light is emitted by plasmonic metals," Nano Lett. **17**, 2568–2574 2017).
23. S. Schietinger, M. Barth, T. Aichele, and O. Benson, "Plasmon-enhanced single photon emission from a nanoassembled metal diamond hybrid structure at room temperature," Nano Lett. **9**, 1694–1698 2009).
24. S. I. Bogdanov, O. A. Makarova, A. S. Lagutchev, D. Shah, C.-C. Chiang, S. Saha, A. S. Baburin, I. A. Ryzhikov, I. A. Rodionov, A. V. Kildishev, A. Boltasseva, and V. M. Shalaev, "Deterministic integration of single nitrogen-vacancy centers into nanopatch antennas," arXiv:1902.05996 2019).
25. I. A. Rodionov, A. S. Baburin, A. R. Gabidullin, S. S. Maklakov, S. Peters, I. A. Ryzhikov, and A. V. Andriyash, "Quantum engineering of atomically smooth single-crystalline silver films," Sci. Rep. **9**, 12232 2019).
26. Y. Wu, C. Zhang, N. M. Estakhri, Y. Zhao, J. Kim, M. Zhang, X.-X. Liu, G. K. Pribil, A. Alù, C.-K. Shih, and X. Li, "Intrinsic optical properties and enhanced plasmonic response of epitaxial silver," Adv. Mater. **26**, 6106–6110 2014).
27. A. F. Koenderink, "On the use of Purcell factors for plasmon antennas," Opt. Lett. **35**, 4208–4210 2010).
28. T. Christensen, W. Yan, A.-P. Jauho, M. Soljačić, and N. A. Mortensen, "Quantum corrections in nanoplasmonics: shape, scale, and material," Phys. Rev. Lett. **118**, 157402 2017).
29. S. Hughes, S. Franke, C. Gustin, M. Kamandar Dezfouli, A. Knorr, and M. Richter, "Theory and limits of on-demand single-photon sources using plasmonic resonators: a quantized quasinormal mode approach," ACS Photon. **6**, 2168–2180 2019).
30. C. Zhang, J.-P. Hugonin, J.-J. Greffet, and C. Sauvan, "Surface plasmon polaritons emission with nanopatch antennas: enhancement by means of mode hybridization," ACS Photon. **6**, 2788–2796 2019).
31. A. Mohtashami and A. F. Koenderink, "Suitability of nanodiamond nitrogen–vacancy centers for spontaneous emission control experiments," New J. Phys. **15**, 043017 2013).
32. M. K. Bhaskar, D. D. Sukachev, A. Sipahigil, R. E. Evans, M. J. Burek, C. T. Nguyen, L. J. Rogers, P. Siyushev, M. H. Metsch, H. Park, F. Jelezko, M. Lončar, and M. D. Lukin, "Quantum nonlinear optics with a germanium-vacancy color center in a nanoscale diamond waveguide," Phys. Rev. Lett. **118**, 223603 2017).
33. N. H. Wan, S. Mouradian, and D. Englund, "Two-dimensional photonic crystal slab nanocavities on bulk single-crystal diamond," Appl. Phys. Lett. **112**, 141102 2018).
34. F. Balzarotti, Y. Eilers, K. C. Gwosch, A. H. Gynnå, V. Westphal, F. D. Stefani, J. Elf, and S. W. Hell, "Nanometer resolution imaging and tracking of fluorescent molecules with minimal photon fluxes," Science **355**, 606–612 2017).
35. R. Faggiani, J. Yang, and P. Lalanne, "Quenching, plasmonic, and radiative decays in nanogap emitting devices," ACS Photon. **2**, 1739–1744 2015).
36. F. Benz, M. K. Schmidt, A. Dreismann, R. Chikkaraddy, Y. Zhang, A. Demetriadou, C. Carnegie, H. Ohadi, B. de Nijs, R. Esteban, J. Aizpurua, and J. J. Baumberg, "Single-molecule optomechanics in "picocavities"" Science **354**, 726–729 2016).
37. K. D. Jahnke, A. Sipahigil, J. M. Binder, M. W. Doherty, M. Metsch, L. J. Rogers, N. B. Manson, M. D. Lukin, and F. Jelezko, "Electron–phonon processes of the silicon-vacancy centre in diamond," New J. Phys. **17**, 043011 2015).
38. I. I. Vlasov, A. A. Shiryaev, T. Rendler, S. Steinert, S.-Y. Lee, D. Antonov, M. Vörös, F. Jelezko, A. V. Fisenko, L. F. Semjonova, J. Biskupek, U. Kaiser, O. I. Lebedev, I. Sildos, P. R. Hemmer, V. I. Konov, A. Gali, and J. Wrachtrup, "Molecular-sized fluorescent nanodiamonds," Nat. Nanotechnol. **9**, 54–58 2014).
39. I. M. Palstra, H. M. Doeleman, and A. F. Koenderink, "Hybrid cavity-antenna systems for quantum optics outside the cryostat?" Nanophotonics **8**, 1513–1531 2019).
40. G. Sun, J. B. Khurgin, and C. C. Yang, "Impact of high-order surface plasmon modes of metal nanoparticles on enhancement of optical emission," Appl. Phys. Lett. **95**, 171103 2009).
41. G. Sun, J. B. Khurgin, and A. Bratkovsky, "Coupled-mode theory of field enhancement in complex metal nanostructures," Phys. Rev. B **84**, 045415 2011).